Applied Catalysis B: Environmental 165 (2015) 519–528

Contents lists available at ScienceDirect

Applied Catalysis B: Environmental

journal homepage: www.elsevier.com/locate/apcatb

Structure sensitivity of selective catalytic reduction of NO with propylene over Cu-doped $Ti_{0.5}Zr_{0.5}O_{2-\delta}$ catalysts

Jie Liu [a], Qidong Zhao [a], Xinyong Li [a,b,c,*], Junhong Chen [b,**], Dongke Zhang [c,**]

[a] Key Laboratory of Industrial Ecology and Environmental Engineering and Key Laboratory of Fine Chemicals, School of Environmental Science and Technology, Dalian University of Technology, Dalian 116024, China
[b] Department of Mechanical Engineering, University of Wisconsin-Milwaukee, Milwaukee, WI 53211, USA
[c] Centre for Energy (M473), The University of Western Australia, 35 Stirling Highway, Crawley, WA 6009, Australia

ARTICLE INFO

Article history:
Received 23 July 2014
Received in revised form
22 September 2014
Accepted 11 October 2014
Available online 30 October 2014

Keywords:
Cu-doped $Ti_{0.5}Zr_{0.5}O_{2-\delta}$
Hierarchical morphology
In situ DRIFTS
Selective catalytic reduction
Structure sensitive

ABSTRACT

The structure sensitivity of selective catalytic reduction (SCR) of NO with propylene over Cu-doped $Ti_{0.5}Zr_{0.5}O_{2-\delta}$ catalysts was investigated systematically in a series of characterizations and *in situ* DRIFT spectroscopy. A Cu-doped $Ti_{0.5}Zr_{0.5}O_{2-\delta}$ catalyst with a hierarchical structure was fabricated successfully using a hydrothermal method (Hy-Sample), and shown to exhibit excellent SCR performance with high reaction rate and turnover frequency (TOF). The physico-chemical properties, mass transfer, and SCR activity of the catalyst depended on the preparation method. Another sample of Cu-doped $Ti_{0.5}Zr_{0.5}O_{2-\delta}$ catalyst prepared using a co-precipitation method (Co-Sample) exhibited a disordered, irregular morphology, whose SCR activity, as determined in a fixed bed reactor, was significantly lower than that of Hy-Sample. In comparison, Hy-Sample possessed an enhanced redox property, and its highly ordered morphology greatly promoted the generation of active sites, including the fine-dispersed CuO species and surface adsorbed oxygen. Consequently, NO and C_3H_6 were readily adsorbed and activated over Hy-Sample and induced the formation of important intermediates with high reactivity, such as isocyanate (−NCO) and cyanide (−CN) species. However, the activation capacity of Co-Sample toward reactants was very weak, and the sequential deficiency of N-containing organics could be the primary reason for the poor SCR activity of Co-Sample.

1. Introduction

Ever-increasing environmental concerns in the last decades have spurred both academic and industrial research, and development effort to devise new methods for elimination of NO_x originating from stationary and mobile sources. For the removal of NO_x from vehicles, selective catalytic reduction of NO_x with hydrocarbons (HC-SCR) is considered as a potential technology from the view of economy, energy-saving and safety as it can eliminate the NO_x and un-burnt hydrocarbons in the exhaust simultaneously [1–3]. However, the current HC-SCR technology is still insufficient for commercial application, and further fine-tuning of catalytic materials is essential to gain satisfactory SCR performance.

As a second generation catalyst support after SiO_2, TiO_2 has been employed commercially in the SCR reactions, such as the well-known catalysts V_2O_5–TiO_2 and V_2O_5 (WO_x or MoO_x)/TiO_2 [4,5]. However, some crystal transformation of TiO_2 occurs at high temperatures, resulting in catalyst deactivation [6]. To enhance the thermal stability of TiO_2, many studies have been carried out. Recently, due to the excellent stability against thermal treatments, ZrO_2 as a doping component has been shown to improve the performance of TiO_2 [7–9]. On the other hand, owning to the ionic radius difference between Zr^{4+} (0.87 Å) and Ti^{4+} (0.64 Å), the partial substitution of Ti by Zr could lead to lattice distortion of TiO_2 and then induce the generation of abundant surface defects. Consequently, the gas-phase NO_x can be more readily adsorbed on the Zr-doped TiO_2 catalysts during the SCR reaction [10–13]. Furthermore, the weak acidic and basic sites on the surface of ZrO_2 also improve the tolerance of catalysts against SO_2 poisoning [6,14,15].

Among the alternatives of active components examined for the low-temperature SCR reaction, copper has been widely explored

* Corresponding author at: Key Laboratory of Industrial Ecology and Environmental Engineering and Key Laboratory of Fine Chemicals, School of Environmental Science and Technology, Dalian University of Technology, Dalian 116024, China. Tel.: +86 41184707733; fax: +86 41184707733.
** Corresponding authors.
E-mail addresses: xinyongli@hotmail.com (X. Li), jhchen@uwm.edu (J. Chen), dongke.zhang@uwa.edu.au (D. Zhang).

http://dx.doi.org/10.1016/j.apcatb.2014.10.038
0926-3373/

due to its efficacy and relatively low cost [16–19]. It is well known that the SCR performance of catalysts depends on the dispersion, nuclearity and oxidation state of the active components, which could be controlled by tailoring catalyst preparation method efficiently [6,12].

In the present study, we designed a new type Cu-doped $Ti_{0.5}Zr_{0.5}O_{2-\delta}$ mixed oxide catalyst using a facile hydrothermal method. The as-prepared catalyst was shown to possess a special hierarchical morphology assembled by hollow spheres. Meanwhile, another sample of Cu-doped $Ti_{0.5}Zr_{0.5}O_{2-\delta}$ mixed oxide was prepared by a co-precipitation method and used as a contrast to investigate the relationship between the properties of catalyst and the synthesis method. A series of physical-chemical characterizations were performed to help reveal the structure sensitivity of the SCR reaction over the Cu-doped $Ti_{0.5}Zr_{0.5}O_{2-\delta}$ catalysts. Moreover, the *in situ* DRIFT spectroscopy was also used to investigate the structure sensitivity of the SCR reaction by examining the reactant adsorption as well as the formation and transformation of intermediates during the SCR process. The findings in this work would contribute to the rational design of SCR catalysts by fine-tuning the surface fabrication.

2. Experimental

2.1. Catalyst preparation

Two Cu-doped $Ti_{0.5}Zr_{0.5}O_{2-\delta}$ catalysts were synthetize using the hydrothermal and co-precipitation methods, respectively. In the hydrothermal process, certain amounts of titanium tetrachloride ($TiCl_4$) and zirconium oxychloride ($ZrOCl_2{\cdot}8H_2O$) were dissolved in deionized water in ice-water bath, and then cupric acetate ($Cu(CH_3COOH)_2{\cdot}2H_2O$), ammonium sulfate ($(NH_4)_2SO_4$) and urea ($CO(NH_2)_2$) were added. After stirring for 2 h, an equal amount of ethanol (EtOH) was added dropwise into the above solution. The molar composition of $TiCl_4$:$ZrOCl_2{\cdot}8H_2O$:$Cu(CH_3COOH)_2{\cdot}2H_2O$:$H_2O$:$(NH_4)_2SO_4$:$CO(NH_2)$:EtOH was controlled to be 1:1:0.16:146:2:36:46. The final mixed solution was then transferred into an autoclave, sealed, heated to and maintained at 95 °C for 24 h. In the co-precipitation process, this same final mixed solution was reflux condensed in a thermostatic oil bath at 95 °C for 24 h. Both slurries obtained in the two methods were filtered after cooling to the room temperature, washed with deionized water and ethanol, and dried at 80 °C for 12 h. The resultant powders were calcinated at 400 °C for 4 h with a heating rate of 2 °C min^{-1}. The Cu-doped $Ti_{0.5}Zr_{0.5}O_{2-\delta}$ samples prepared using the hydrothermal and co-precipitation methods were labeled as Hy-Sample and Co-Sample, respectively. Moreover, to investigate the high-temperature treatment effect on Hy-Sample, another two samples were prepared by hydrothermal method also, and these samples were calcinated at 600 and 800 °C for 4 h, respectively, by the same heating rate of 2 °C min^{-1}.

2.2. Characterization

The exact copper content in the samples was determined with an inductively coupled plasma atomic emission spectrometer (ICP-AES, Perkin-Elmer Optima 3300 DV apparatus). The specific surface area, pore volume and average pore diameter of catalyst were measured using physical adsorption of N_2 at −196 °C with NOVA 1200 (Quanta Chrome). The catalyst morphology was characterized by scanning electron microscope (SEM, FEI-Quanta 450), transmission electron microscope (TEM, FEI-TECNAI G20), and high-resolution transmission electron microscopy (HR-TEM, FEI-TECNAI G20). Electron paramagnetic resonance (EPR) analysis was performed at room temperature using a Bruker (A200-9.5/12) operating at the X band (~9.8 GHz). The magnetic field was modulated at 100 kHz and the *g* value was determined from the precise frequency and magnetic field values. Hydrogen-temperature programed reduction (H_2-TPR) analysis was carried out on a Chembet PULSAR TPR/TPD (p/n 02139-1), and the H_2 consumption in the effluent was monitored with a TCD detector. X-ray photoelectron spectra (XPS) were recorded using a Thermo ESCALAB 250XI electron spectrometer. Binding energies of Cu 2p, O 1s and Zr 3d were calibrated using C 1s (BE = 284.8 eV) as a standard.

2.3. Catalytic test

The SCR activity measurement was carried out in a fixed-bed quartz tube reactor (6 mm internal diameter) containing 200 mg catalyst (40–60 mesh). Prior to an experiment, the catalyst was pretreated at 250 °C for 1 h in an Ar stream, and the activity test was performed from 150 °C to 450 °C at a heating rate of 10 °C min^{-1}. The typical reactant gas composition was as follows: 1000 ppm NO, 1000 ppm C_3H_6, 10 vol.% O_2, 10 vol.% H_2O (when used) and 100 ppm SO_2 (when used), with He as balance. The total flow rate was 100 ml min^{-1}, which corresponded to an hourly space velocity (GHSV) of approximately 30,000 h^{-1}. The concentrations of NO, NO_2 and CO in the inlet and outlet gases were measured using a chemiluminescence gas analyzer (Testo 350). The concentrations of N_2, N_2O and C_3H_6 were analyzed using a gas chromatograph (Agilent 7890 A), and the corresponding columns were 5A molecular sieve and Paropak Q columns with a thermal conductivity detector (TCD) and a 6X-104D column with a flame ionization detector (FID), respectively.

The NO conversion, C_3H_6 conversion, NO_2 yield, N_2 yield, N_2O yield and CO yield were calculated as follows:

$$\text{NO conversion} = \frac{[NO]_{in} - [NO]_{out}}{[NO]_{in}} \times 100\% \quad (1)$$

$$C_3H_6 \text{ conversion} = \frac{[C_3H_6]_{in} - [C_3H_6]_{out}}{[C_3H_6]_{in}} \times 100\% \quad (2)$$

$$NO_2 \text{ yield} = \frac{[NO_2]}{[NO]_{in}} \times 100\% \quad (3)$$

$$N_2 \text{ yield} = \frac{[N_2] \times 2}{[NO]_{in}} \times 100\% \quad (4)$$

$$N_2O \text{ yield} = \frac{[N_2O] \times 2}{[NO]_{in}} \times 100\% \quad (5)$$

$$\text{CO yield} = \frac{[CO]/3}{[C_3H_6]_{in}} \times 100\% \quad (6)$$

The reaction rate and turnover frequency (TOF) for NO conversion were calculated according to the following equations:

$$R_{NO} = X_{NO}\nu/m_{cat}/S_{BET}\,(\text{mol s}^{-1}\,\text{m}^{-2}) \quad (7)$$

$$\text{TOF} = \frac{(P_v/R_T)X_{NO}}{m_{cat}\beta_{Cu}/M_{Cu}} \cdot (\text{s}^{-1}) \quad (8)$$

where X_{NO} (%) is the NO conversion, ν (mol s^{-1}) the flow rate of NO, m_{cat} (g) the mass of the catalyst, S_{BET} (m^2 g^{-1}) the BET specific surface area, *P* the standard atmospheric pressure (1.01×10^5 Pa), *R* the proportional constant (8.314 J mol^{-1} K^{-1}), *T* (K) the reaction temperature, β_{Cu} (%) the Cu loading calculated from the XPS spectra, and, finally, M_{Cu} the molar mass of Cu (63.54 g mol^{-1}).

2.4. In situ DRIFT study

In situ DRIFT spectra were recorded using an FTIR spectrometer (Bruker VERTEX 70-FTIR) equipped with a liquid-N_2-cooling high-sensitivity MCT detector and DRIFT cell. Prior to each experiment, the sample (~50 mg) was pretreated in He stream (50 ml min^{-1})

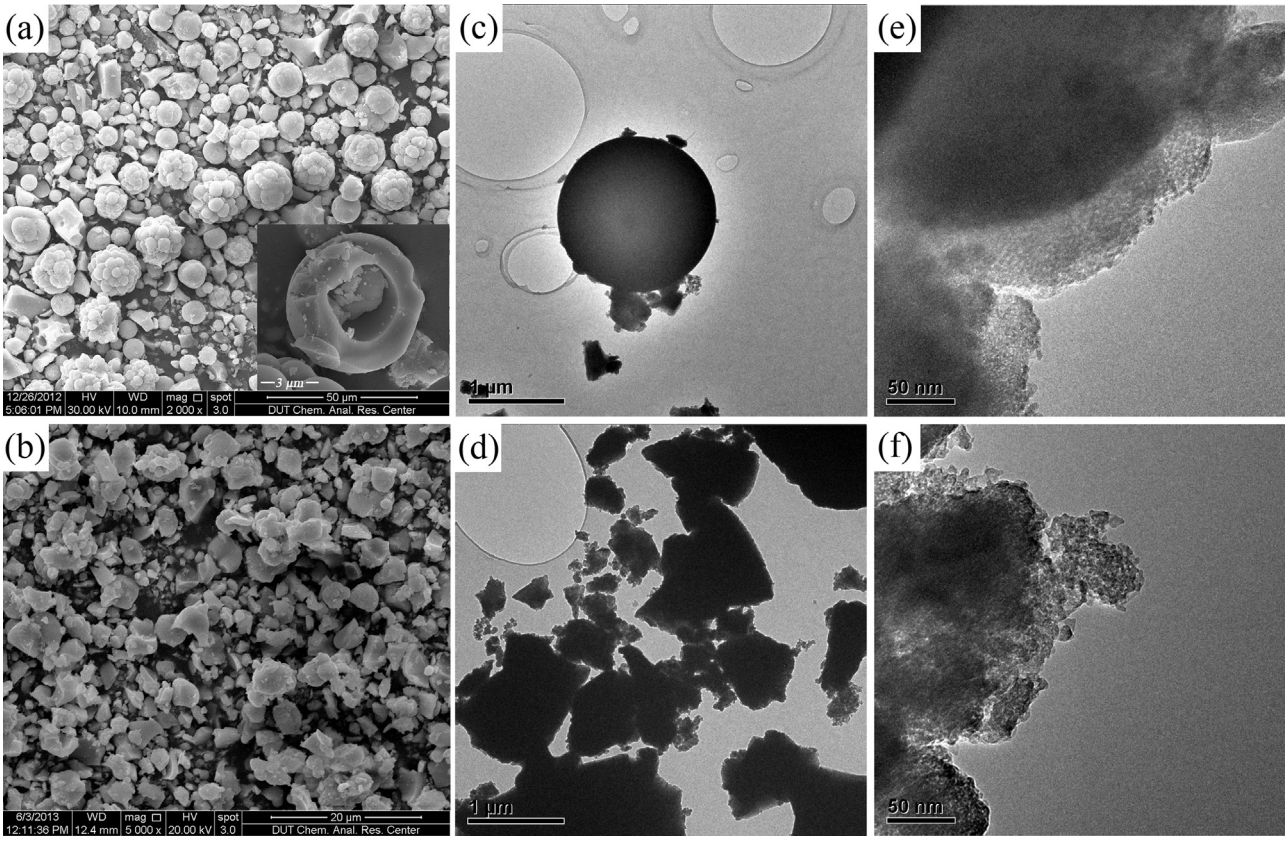

Fig. 1. SEM images of as-prepared Hy-Sample (a) and Co-Sample (b), and TEM images of Hy-Sample (c and e) and Co-Sample (d and f).

at 250 °C for 1 h to remove the moisture, and then cooled to the desired temperature. All spectra were recorded over accumulative 64 scans with a resolution of 4 cm^{-1} in the range of 4000–400 cm^{-1}. The concentrations of NO, C_3H_6, and O_2 in the gas mixture were 1000 ppm, 1000 ppm, and 10 vol.%, respectively, with He as balance, and the flow rate of mixed gas was 50 ml min^{-1}.

3. Results and discussions

3.1. Characterizations of catalysts

3.1.1. Morphology and physical properties

Fig. 1 displays the SEM and TEM graphs of Hy-Sample and Co-Sample, and the role of preparation methods in the controlling of surface topography could be better understood. As presented in Fig. 1a, Hy-Sample had a rough surface with hierarchical morphology which was assembled by several spheres of diverse size. Combining the SEM image of a broken sphere (the insert in Fig. 1a) and the TEM photo of the sphere in Hy-Sample (Fig. 1c), the spheres were considered to have a hollow structure. In contrast, the morphology of Co-Sample was disordered and irregular, as described in Fig. 1b and d. From the TEM images presented in Fig. 1e and f, it was clearly that both Hy-Sample and Co-Sample were assembled by little particles, and the particles in Hy-Sample possessed much better dispersion and smaller size, which suggested that the hydrothermal process inhibited the agglomeration of particles efficiently.

The specific surface area (S_{BET}), pore volume as well as average pore diameter of Hy-Sample and Co-Sample are presented in Table 1. The BET surface area and pore volume of Hy-Sample were 14.45 $m^2 g^{-1}$ and 0.047 $cm^3 g^{-1}$, respectively. By comparison, the specific surface area and pore volume of Co-Sample were increased to 91.07 $m^2 g^{-1}$ and 0.077 $cm^3 g^{-1}$, respectively. The pore diameter of Hy-Sample was 9.61 nm and larger than that of Co-Sample, which was only 3.33 nm.

3.1.2. XPS studies

XPS characterization has been performed to gain detailed insight about the atomic concentrations and valence states of Cu, O, Zr elements over Hy-Sample and Co-Sample. The Cu 2p spectra are presented in Fig. 2a and separated into 7 peaks by peak-fitting deconvolution. The Cu^{2+} species are characterized by a Cu $2p_{3/2}$ binding energy of 933.9 eV with a shake-up or satellite peak located at 938.5–946.5 eV, and the binding energy at 931.9 eV is assigned to Cu^+ [12,20]. The surface concentrations of Cu^+ and Cu^{2+} in molar ratio over Hy-Sample and Co-Sample are presented in Table 2, where the relative amount of Cu^+ is measured by the area ratio of peak 1 to peaks 1–4, and the sum of the relative amount of Cu^+ and Cu^{2+} is 100% [20]. As presented in Table 2, the surface concentration of Cu^{2+} over Hy-Sample was 93.8% and higher than that of 81.7% over Co-Sample. Dong et al. reported that the chemisorbed NO occurred on the Cu^{2+} species [12], and the Cu^{2+}-O^- or Cu^{2+}-O^{2-} species were considered as the active sites in HC-SCR reaction in the study of Iwamoto et al. [21]. Furthermore, the surface concentration of Cu over Co-Sample was only 1.45%, much lower than that of 2.61% over Hy-Sample, though the Cu concentrations in Hy-Sample and Co-Sample measured by ICP were similar, which were 4.671% and 5.005% (wt%), respectively. Herein, it was speculated that the

Table 1
Structural parameters of Hy-sample and Co-Sample.

Samples	S_{BET} ($m^2 g^{-1}$)	Pore volume ($cm^3 g^{-1}$)	Average pore diameter (nm)
Hy-Sample	14.45	0.047	9.61
Co-Sample	91.07	0.077	3.33

Table 2
Surface chemical states and quantitative results of surface atomic concentration (% in molar ratio) over Hy-sample and Co-Sample derived from XPS data.

Samples	Cu[a] (%)	Ti[a] (%)	Zr[a] (%)	O[a] (%)	Cu^{2+} [b] (%)	Cu^{+} [b] (%)	O_A (%)	O_L (%)	O_A/O_L
Hy	2.61	9.43	11.69	76.26	93.8	6.2	57.9	42.1	1.38
Co	1.45	11.97	12.96	73.62	81.7	18.3	45.6	54.4	0.84

[a] mol%.
[b] $Cu^{2+} + Cu^{+} = 100\%$.
The concentration of Cu in Hy-Sample and Co-Sample obtained by ICP was 4.671% and 5.005% (wt%) respectively.

co-precipitation process made more Cu species be coated in the interior of material and covered by the layer of TiO_2–ZrO_2 mixed oxide, and consequently led to some loss of CuO_x active sites.

The XPS spectra of O 1s are displayed in Fig. 2b. The sub-band at 531.4 eV corresponds to the surface adsorbed oxygen (denoted as O_A), such as O_2^{2-} or O^- belonging to defect oxide or hydroxyl-like group, and the sub-band at 530.0 eV is attributed to the lattice oxygen O^{2-} (denoted as O_L) [22–24]. From the quantitative peak-fitting results of O 1s presented in Table 2, it was suggested that the hydrothermal method benefited the generation of adsorbed surface oxygen O_A, and the O_A ratio over Hy-Sample was 57.9%, higher than that of 45.6% over Co-Sample. Due to the much higher mobility of O_A compared with that of O_L, the catalyst with higher O_A ratio could be more active in the oxidation reaction. Moreover, due to the unsaturation, the surface adsorbed oxygen (O_2^{2-} and O^- species) could act as the electron accepter and easily react with gas-phase NO with one-electron bond, and this deduction was in agreement with previous reports [25,26]. Herein, the Hy-Sample with higher O_A ratio may provide more adsorption sites for gas-phase NO, and the oxidation of NO to NO_2 as well as the subsequent formation of surface-adsorbed nitrates could be more easily and quickly. As the NO activation was widely accepted as an important step in SCR reaction [7,27], the catalytic activity of Hy-Sample could be promoted, and this speculation could be confirmed by *in situ* DRIFT results below. On the other hand, the ratio of O_A/O_L was a common way to roughly assess the amount of oxygen vacancies [28]. The O_A/O_L ratio over Hy-Sample and Co-Sample was 1.38 and 0.84, respectively, suggesting that the hydrothermal method facilitated the formation of oxygen vacancies on the catalyst surface, and therefore promoted the adsorption of gas-phase O_2 on the catalyst surface.

Fig. 2c illustrates the XPS spectra of Zr 3d. For the Hy-Sample, the binding energy of Zr photoelectron peaks centered at 182.5 and 184.9 eV, which were assigned to Zr $3d_{5/2}$ and Zr $3d_{3/2}$, respectively, and indicated the oxidation state 4+ of Zr over Hy-Sample [11]. By comparison, the Zr $3d_{5/2}$ and Zr $3d_{3/2}$ over Co-Sample shifted to the lower binding energy slightly, and centered at 182.3 and 184.7 eV, respectively, indicating the possible presence of the reduced Zr species [29].

3.1.3. *Paramagnetic defects and redox behavior of catalysts*

EPR spectroscopy is extensively used to probe and elucidate the structural environmental of paramagnetic species and their interactions, and the EPR spectra of Hy-Sample and Co-Sample obtained at room temperature are depicted in Fig. 3. Both of the two catalysts showed an isotropic signal with $g = 2.139$ and no resolvable splitting, suggesting the existence of isolated ion Cu^{2+} [30,31], and Cu^{2+} species were considered responsible for the dominant contribution to the spectra. Besides, there was another symmetric signal over Co-Sample resonating at $g = 2.005$. According to references [3,32], this signal corresponded to the superoxide species chemisorbed on titanium or zirconium cations (O_2^-–Ti^{4+} or O_2^-–Zr^{4+} species). As presented in Table 1, the hydrothermal method led to a significant loss of surface area. Due to the small surface area, partial encapsulation of titanium or zirconium cations may occur over Hy-Sample, and therefore prevent the accessibility of catalyst to O_2, which could be the reason for the absence of the free electron signal ($g = 2.005$) over Hy-Sample. Similar deductions have also been reported by Fernández-García et al. [33].

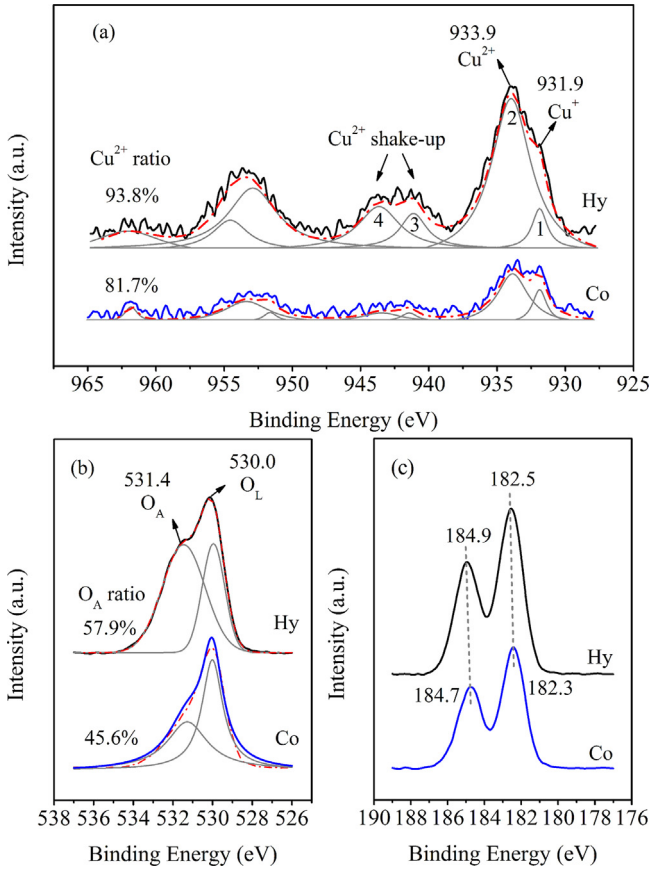

Fig. 2. XPS spectra of Cu 2p (a), O 1s (b), and Zr 3d (c) for Hy-Sample and Co-Sample.

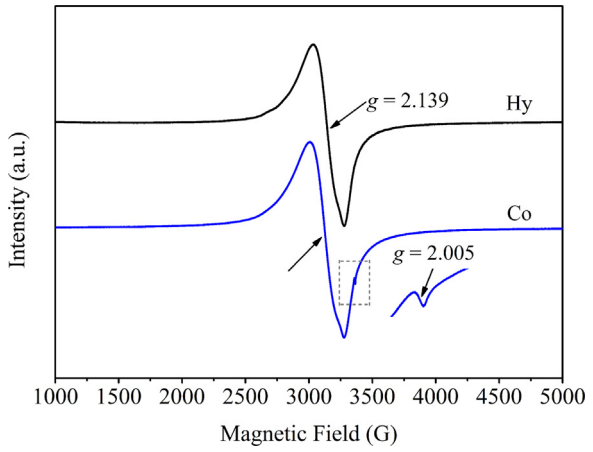

Fig. 3. EPR spectra of Hy-Sample and Co-Sample.

Table 3
Quantitative analysis of H_2-TPR for Hy-Sample and Co-Sample.

Sample	H_2 consumption (mmol/g)						H_2/Cu (mmol/mmol)
	α	β	γ	δ	λ	Total	
Hy-Sample	0.08	0.41	0.54	–	–	1.03	1.31
Co-Sample	–	–	–	3.83	4.64	8.47	–

H_2-TPR experiment has been performed to examine the effect of synthesis method on the reducibility of catalyst. The H_2-TPR profiles of Hy-Sample and Co-Sample and the corresponding quantitative analysis are presented in Fig. 4 and Table 3, respectively. Based on the different reducibility of various copper oxide species, the H_2-TPR profile of Hy-Sample in the temperature range of 100–400 °C was divided into three peaks by Gaussian method. According to literatures [8,34], α, β and γ reduction peaks centered at 222, 250 and 287 °C, respectively, were attributed to the reduction of highly dispersed CuO, small two- and three-dimensional clusters of CuO, and large bulk CuO particles, respectively. As the presence of Cu^+ was confirmed by XPS result, the reduction from $Cu^+ \rightarrow Cu^0$ could not be excluded totally, and the characteristic peak may be overlapped with that of various CuO particles. By comparison, the reduction peak of CuO species over Co-Sample was very different from that of Hy-Sample, which only exhibited a shoulder band with pretty weak intensity at a much higher temperature around 350 °C. Herein, the reducible CuO species in Co-Sample existed as a bulk form, and the distinct decrease in the quantity of reducible CuO species could be attributed to the serious coating of CuO species in the interior of material, which was consistent with the XPS results. Moreover, based on the theory that the lager particle size, the higher reduction temperature [16], the co-precipitation method not only deceased the reducibility of CuO species, but also enlarged the particle size of CuO significantly.

Further increasing the reduction temperature from 400 to 800 °C, the signal over Hy-Sample appeared white until the end, whereas there were two reduction peaks over Co-Sample. The broad peak δ (548 °C) and the intense sharp peak λ (725 °C), were assigned to the reduction of adsorbed oxygen and the release of bulk oxygen, respectively [11,35,36]. From the quantitative analysis of H_2-TPR, the value of H_2/Cu ratio over Hy-Sample was 1.31 and higher than the theoretical value of 1.0, which corresponded to the complete reduction from Cu^{2+} to Cu^0. Herein, the H spillover effect occurred over Hy-Sample, and the excessive hydrogen consumption was attributed to the reduction of surface adsorbed oxygen.

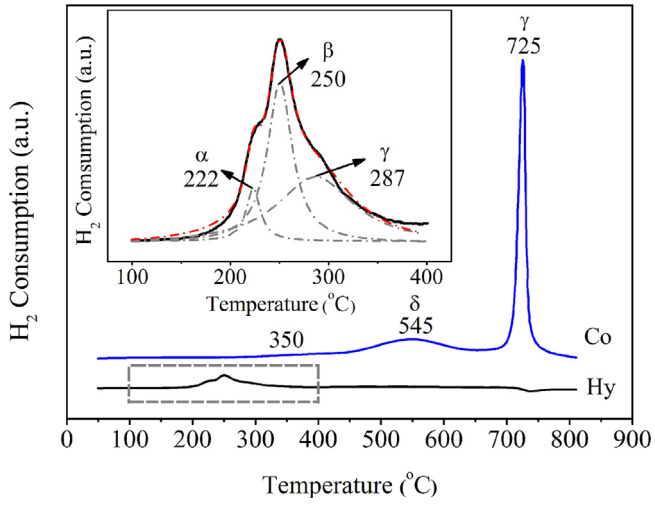

Fig. 4. H_2-TPR profiles of Hy-Sample and Co-sample. (Inset: the enlarged H_2-TPR profiles of the Hy sample in the temperature range of 100–400 °C).

Due to the assistance of CuO_x species, the reduction of surface adsorbed oxygen shifted to a lower temperature and led to the overlap of δ peak with the reduction peaks of CuO_x species. Similar to the study of Song et al. [11], the absence of λ reduction peak over Hy-Sample may be attributed to the higher oxygen deficiency as discussed in Section 3.1.2. Moreover, the encapsulation of titanium or zirconium cations in Hy-Sample caused by the loss of surface area, may also prevent the accessibility of catalyst to H_2 during TPR experiment, and therefore decreased the feasibility of bulk oxygen reduction. According to H_2-TPR analysis, it was deduced that the hydrothermal method enhanced the reduction potential of CuO_x species as well as the surface adsorbed oxygen, and this seemed to be beneficial for the promotion of SCR activity.

3.1.4. *The relationship between morphology and chemical properties of catalyst*

The formation mechanism of the hierarchical structure morphology of Hy-Sample is illustrated in Fig. 5. Firstly, mixed metal hydroxide particles with poor crystallinity were formed by the sequential hydrolysis of urea and metal cations (Cu^{2+}, Ti^{4+} and Zr^{4+}). Owning to the high surface energy of these little particles and the high affinity of SO_4^{2-} to bridge polymeric hydroxylated metal complex, the hydroxide transformed from featureless amorphous material to the regular and solid spheres (Step II). This phenomenon also occurred in the formation of boehmite and TiO_2 hollow microspheres reported by Yu and Chen respectively [37,38]. After that the hollow spheres were formed during the Ostwald ripening process, as described in Step III. In this step, the external surface of the spherical particles was protected by surface adsorbed SO_4^{2-}, thus the formation of hollow spherical morphology based on the progressive dissolution and redistribution of matter from the interior to exterior processed smoothly [37]. Finally, due to the high pressure during the hydrothermal process, these hollow spheres aggregated and formed the material with hierarchical structure.

For the co-precipitation process, alcohol evaporated quickly at 95 °C though it returned by reflux condensation. Since $(NH_4)_2SO_4$ was soluble in water and insoluble in alcohol [39], the sequential evaporation of alcohol led to the sustaining changes of the solubility and distribution of $(NH_4)_2SO_4$ in the suspension, which was a dynamic equilibrium. Herein, the formation of spherical particles in step III could not be well protected by SO_4^{2-} as that in the hydrothermal process. Subsequently, the Ostwald ripening process was destroyed and the particles aggregated randomly, leading to the formation of irregular morphology of Co-Sample. More importantly, this irregular aggregation resulted in the coating of copper species in the center of these bulk particles (Fig. 1b). Then the molar concentration of Cu on the catalyst surface was decreased and the reducibility of CuO was inhibited at the mean time, which would reduce the amount of active sites participating in the SCR reaction.

3.2. *Kinetic results of NO reduction by C_3H_6*

To elucidate the intrinsic catalytic activity of Hy-Sample and Co-Sample, the activity test of SCR reaction was performed, and the reaction rate and TOF on the basis of NO conversion were calculated using Eqs. (7) and (8), respectively. The conversions of reactants (NO and C_3H_6) and yields of products (N_2, NO_2, N_2O and CO) depending on reaction temperatures are presented in Fig. 6a–c. The

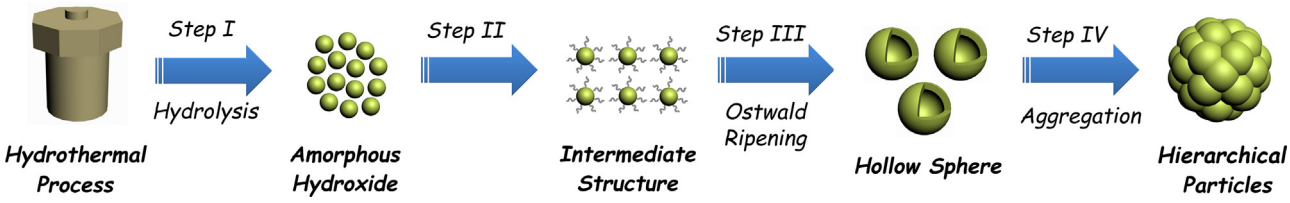

Fig. 5. Schematic illustration of the morphology evolution for flower-like structure assembled by hollow spheres during hydrothermal process.

production profiles suggested that the SCR activity of Hy-Sample was much higher than that of Co-Sample. As presented in Fig. 6a, Hy-Sample exhibited a better low-temperature activity, obtaining the maximum NO conversion of 68.8% at 275 °C, while the maximum NO conversion over Co-Sample was only 29.5% and was obtained at a much higher temperature of 425 °C. The NO_2 yield over Hy-Sample was so low as to be ignorable, while a higher NO_2 yield was obtained over Co-Sample at high temperature, achieving the maximum of 11.4% at 425 °C. Fig. 6b compared the N_2 and N_2O yield over these two samples, which indicated the much higher catalytic activity of Hy-Sample from the view of N_2 yield, as well as its negligible N_2O yield during the SCR reaction. The C_3H_6 conversion and CO yield are depicted in Fig. 6c. It was clear that the C_3H_6 oxidation over Co-Sample was much weaker compared with that of Hy-Sample, and the obvious C_3H_6 conversion (~26%) began at a much higher temperature of 350 °C. Meanwhile, the incomplete oxidation of C_3H_6 over Co-Sample was more obvious, resulting in a higher CO yield. Combining the product profiles, it was suggested that the unsatisfactory performance of Co-Sample was mainly attributed to its poor capacity in the C_3H_6 oxidation, which restrained the formation of derivative from C_3H_6 activation and led to the lack of active species participating in the NO reduction. Moreover, these results suggested that as a new type of metal oxide catalyst, the Hy-Sample was a better low-temperature catalyst compared with Ag/Al_2O_3, which was the most widely studied catalyst used for HC-SCR reactions. Generally speaking, the NO conversion or N_2 yield of Ag/Al_2O_3 is less than 50% when the reaction temperature is below 400 °C, and a lower temperature of 300 °C may even lead to the inertness of catalyst in the reduction of NO [40–42].

Fig. 6d and e presents the Arrhenius-type plot for the reaction rate and TOF as the function of reaction temperatures. For Hy-Sample, the reaction rate and TOF had a positive relationship with the reaction temperature in the range of 150–275 °C (2.36–1.82 K^{-1}), while the values were decreased with the further increase of temperature. The decline of reaction rate and TOF at high temperature was attributed to the enhancement of the combustion of C_3H_6, which was considered as the primary side reaction

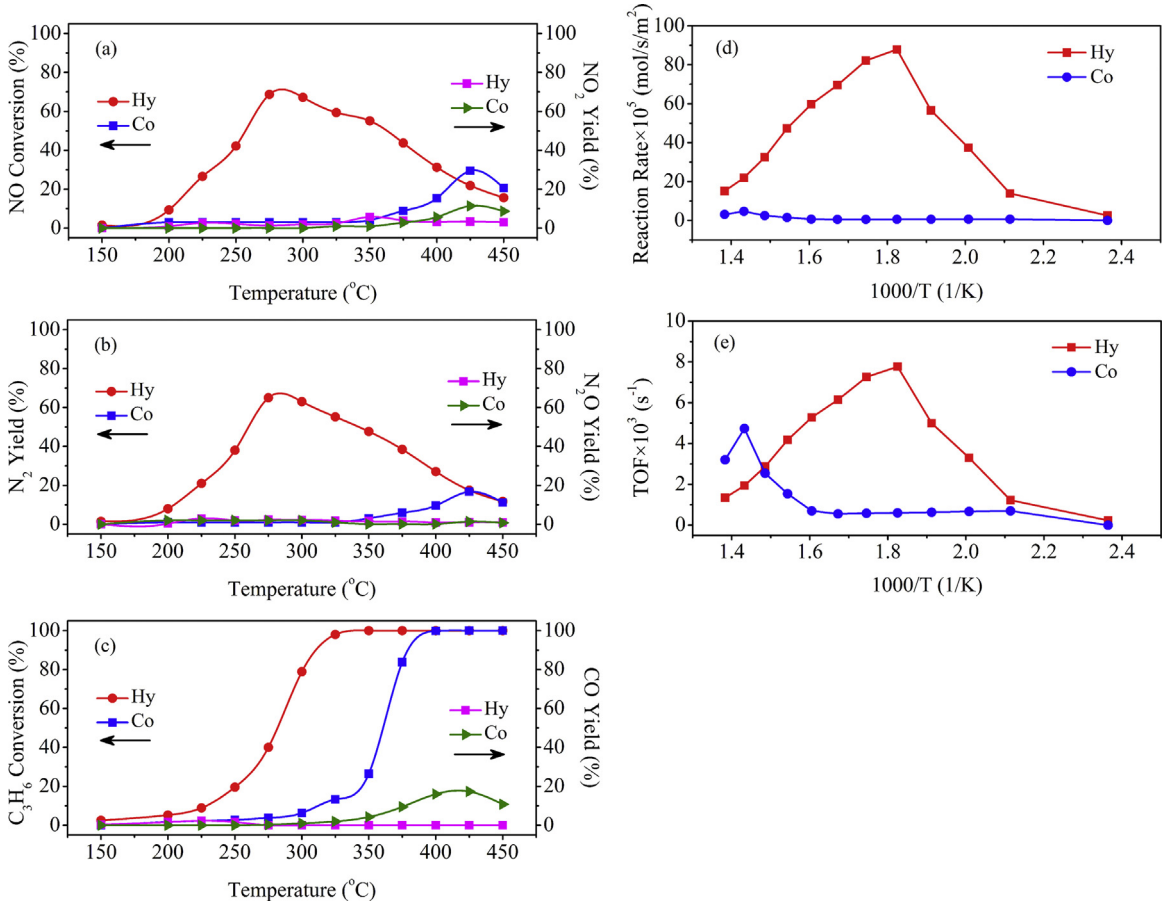

Fig. 6. C_3H_6-SCR performance of Hy-Sample and Co-Sample depended on reaction temperatures. (a) NO conversion and NO_2 yield, (b) N_2 and N_2O yield, (c) C_3H_6 conversion and CO yield, (d) reaction rates of NO conversion, and (e) TOF value of NO conversion. Reaction conditions: [NO] = [C_3H_6] = 1000 ppm, [O_2] = 10 vol.%, He as balance.

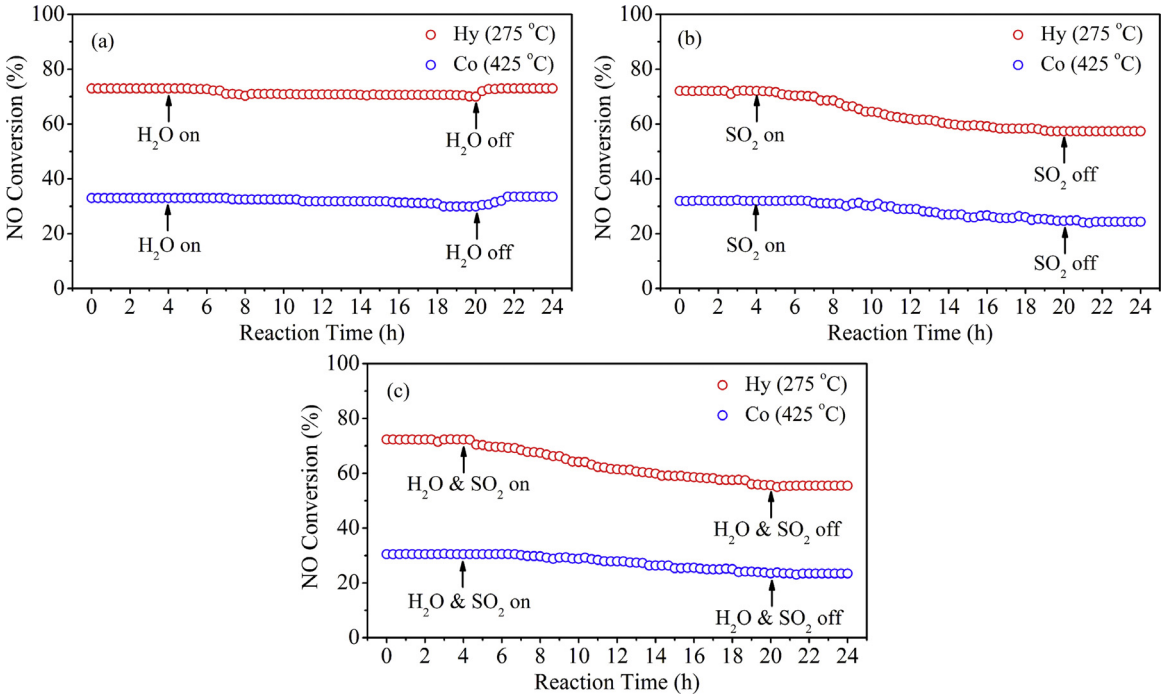

Fig. 7. Influence of H_2O, SO_2 and the co-existence of H_2O and SO_2 on NO conversions of Hy-Sample at 275 °C and Co-Sample at 425 °C. Reaction conditions: [NO] = [C_3H_6] = 1000 ppm, [O_2] = 10 vol.%, [H_2O] = 10 vol.% (when used), and [SO_2] = 100 ppm (when used), with He as balance.

in HC-SCR. However, the reaction rate and TOF over Co-Sample were pretty low in the whole temperature range, though there was a slight elevation at high temperature above 350 °C. According to the kinetic results of NO reduction, it was suggested that though the co-precipitation method endowed the catalyst with higher surface area (91.07 $m^2\,g^{-1}$), it could not provide enough efficient active sites responsible for the SCR reaction. In contrast, the hydrothermal method was an appropriate synthesis method to improve the physical-chemical properties of catalyst, which promoted the mass transfer, the reaction rate and the TOF of catalyst. The effect of synthesis methods on the activation of reactants and the formation of intermediates would be investigated by *in situ* DRIFTS spectra below.

Fig. 7a presents the effect of H_2O on the *de*NO_x efficiency of Hy-Sample and Co-Sample. Both Hy-Sample and Co-Sample exhibited a high H_2O-resistance capacity. The addition of H_2O to the feeding gas led to almost no change of NO conversion of catalysts (275 °C for Hy-Sample and 425 °C for Co-Sample, respectively). This result is consistent with previous works reported by Shimizu and Pérez-Ramírez et al. [43–45], which suggested that the water addition usually had no significant effect on the NO reduction when the short chain hydrocarbons were used as reductants. Whereas by increasing the carbon number of hydrocarbons, the presence of H_2O may lead to a dominant effect on the HC-SCR reactions, which is usually a promotion effect. According to previous reports, the activity of *n*-octane-SCR reaction could be elevated by the introduction of H_2O, because the *n*-octane oxidation by O_2 as well as the poisoning effect caused by carboxylate and carbonate species were suppressed markedly in the H_2O-containing case [43,46].

As the permanent existence of SO_2 in typical diesel fired exhausts may cause a deactivation of catalyst, the NO conversions over Hy-Sample and Co-Sample in the presence of SO_2 as well as in the co-existence of H_2O and SO_2 have also been measured, and the results are displayed in Fig. 7b and c, respectively. As presented in Fig. 7b, the introduction of SO_2 led to an irreversible decrease of NO conversions for both samples, which were approximately decreased by 17% and 8%, respectively. In the H_2O and SO_2-containing case (Fig. 7c), the catalysts exhibited a similar performance to that in the SO_2-containing reaction, though a slightly further decline of NO conversion was observed over the two catalysts. As both the Hy-Sample and Co-Sample exhibited an excellent H_2O-resistance, the presence of SO_2 was considered as the major factor for the deactivation of catalysts. Moreover, the long-term test and high-temperature treatment for Hy-Sample have also been carried out to investigate its catalytic performance more comprehensively, and the results are displayed in Figs. S1 and S2, respectively. The measurement results indicated that Hy-Sample (calcinated at 400 °C) could keep an excellent stability for 72 h at 275 °C, but a high calcination temperature of 800 °C led to a significant deactivation of catalyst.

Supplementary Figs. S1 and S2 related to this article can be found, in the online version, at http://dx.doi.org/10.1016/j.apcatb.2014.10.038.

3.3. *In situ* DRIFTS studies

3.3.1. *NO and O_2 co-adsorption*

Fig. 8a and b presents the DRIFTS spectra of surface adsorbed species formed by the co-adsorption of NO + O_2 with respect to the reaction temperature over Hy-Sample and Co-Sample catalysts, respectively. On the surface of Hy-Sample, the primary adsorbed species at room temperature were various nitrates, including monodentate nitrates (1290 and 1493 cm^{-1}), bidentate nitrates (1251, 1544 and 1580 cm^{-1}), and bridging nitrates (1228 and 1611 cm^{-1}) [4]. The band centered at 1448 cm^{-1} was assigned to monodentate nitrite species or *trans*-N_2O_2 formed by the dimerization of NO molecules [47], and the band around 1700 cm^{-1} was assigned to N_2O_4 species due to NO_2 dimerization [48]. For Co-Sample, though the characteristic bands attributed to monodentate, bidentate, bridging nitrates, NO_2 and N_2O_4 were also detected, the intensity of them was much weaker than that over Hy-Sample. Besides, there were some differences between the DRIFT spectra of Hy-Sample and those of Co-Sample, including the appearance of some new bands (1376, 1626 and 1682 cm^{-1}) and the absence

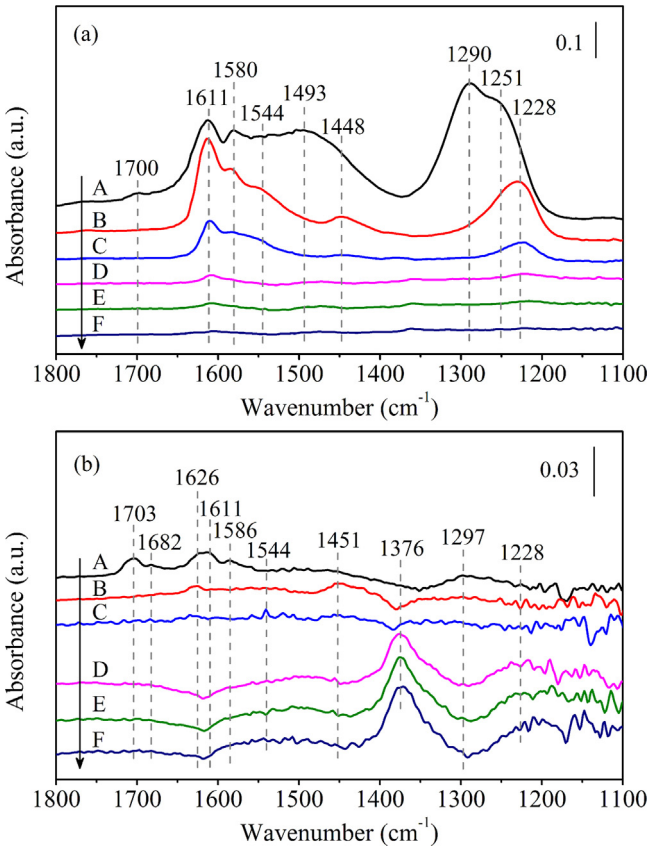

Fig. 8. *In situ* DRIFT spectra of the species deriving from NO + O_2 co-adsorption over Hy-Sample (a) and Co-Sample (b) at different temperatures. (A) 25 °C, (B) 150 °C, (C) 200 °C, (D) 250 °C, (E) 275 °C and (F) 300 °C.

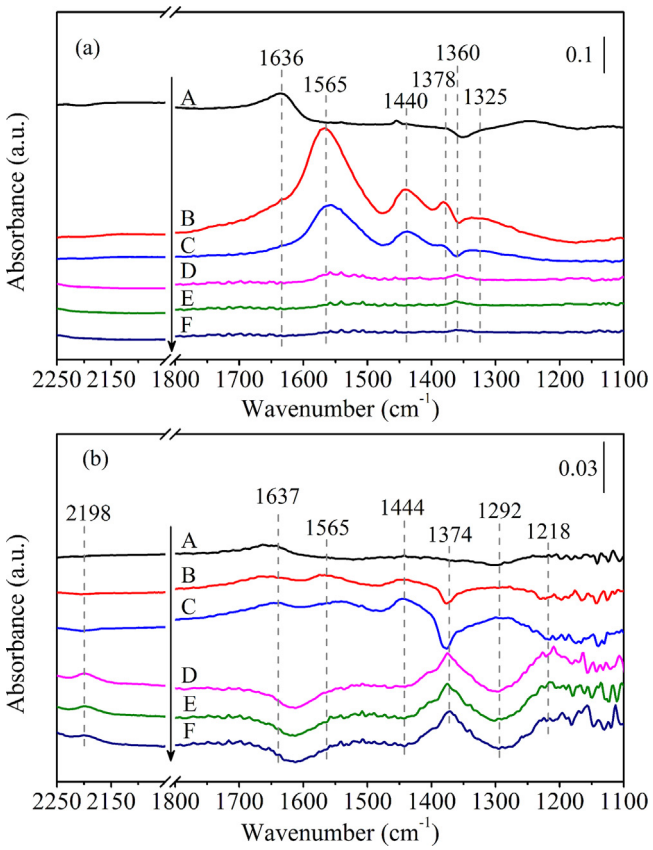

Fig. 9. *In situ* DRIFT spectra of the species deriving from C_3H_6 + O_2 co-adsorption over Hy-Sample (a) and Co-Sample (b) at different temperatures. (A) 25 °C, (B) 150 °C, (C) 200 °C, (D) 250 °C, (E) 275 °C and (F) 300 °C.

of the bands centered at 1251 and 1493 cm^{-1}. The pair of bands 1376 + 1682 cm^{-1} was assigned to N_2O_4, and the band at 1626 cm^{-1} was attributed to the mixed band overlapped by the bridging nitrates and the adsorbed NO_2 on oxide surface [4,16,48]. With increasing the reaction temperature, the intensity of these characteristic bands was decreased gradually over both Hy-Sample and Co-Sample.

According to the *in situ* DRIFT spectra presented in Fig. 8, it was suggested that the catalyst synthesis method changed the types of main adsorbed species on the catalyst surface. The primary species deriving from NO + O_2 co-adsorption over Hy-Sample were nitrates with different configurations, while those over Co-Sample were NO_2 and N_2O_4 with pretty low quantity. It was well known that the nitrates derived from NO_2 adsorbed on basic oxygen sites, which were formed by the NO oxidation [49,50]. As mentioned above, Hy-Sample possessed abundant surface adsorbed oxygen with high mobility and reactivity, including oxygen defects and hydroxyl-like group. Herein, NO_2 was readily conversed to nitrates on the surface of Hy-Sample, while this transformation could not occur efficiently over Co-Sample.

3.3.2. C_3H_6 and O_2 co-adsorption

The DRIFTS spectra of the species deriving from C_3H_6 + O_2 co-adsorption at various temperatures over Hy-Sample and Co-Sample are presented in Fig. 9a and b, respectively. The main adsorbed species over Hy-Sample at room temperature (25 °C) was the gas-phase C_3H_6, showing a characteristic band centered at 1636 cm^{-1}, which was assigned to the C=C stretching [51]. The activation of C_3H_6 occurred when the temperature was increased to 150 °C, leading to some new bands appeared at 1565, 1440 and 1378 cm^{-1}. The bands centered at 1565 and 1440 cm^{-1} were assigned to ν_{as}(OCO) and ν_s(OCO) of acetate species, and the bands around 1378 and 1327 cm^{-1} were attributed to δ(CH) of formate species and δ(CH) of enolic species [52,53]. With the further increase of reaction temperature, the band at 1378 cm^{-1} shifted to a lower wavenumber of 1360 cm^{-1}. Meanwhile, the complete oxidation from oxygenated species to CO_2 was enhanced, and the intensity of the referred bands was decreased gradually until vanished above 275 °C.

For Co-Sample, besides the characteristic bands of gas-phase C_3H_6, acetate and formate, a new band was detected on the catalyst surface, which centered at 1292 cm^{-1} and was attributed to the acrylate species [52]. Compared with Hy-Sample, the concentrations of C_3H_6 derivative over Co-Sample were much lower, and the formate (1374 cm^{-1}) was generated at a much higher temperature of 250 °C. Herein, it was suggested that Co-Sample had a poor capacity toward C_3H_6 activation, and this could be a primary reason for its unsatisfied SCR performance. Moreover, on the surface of Co-Sample, there was a new band appeared when the reaction temperature was above 250 °C, which centered at 2198 cm^{-1} and was assigned to the stretching vibrations of CO admolecule [51]. The generation of CO was caused by the incomplete oxidation of C_3H_6 or oxygenates.

3.3.3. SCR process

The formation and transformation of surface adsorbed species depending on the reaction temperatures over Hy-Sample and Co-Sample during SCR process have also been investigated by DRIFTS spectra, and the results are presented in Fig. 10a and b, respectively. During exposure of Hy-Sample in NO + C_3H_6 + O_2 mixed gas flow at 25 °C, the catalyst surface was covered by monodentate (1290 and 1485 cm^{-1}), bidentate (1254 and 1580 cm^{-1}), bridging (1613 cm^{-1}) nitrates, and chemisorbed NO (1867 cm^{-1}) [16,54]. When the

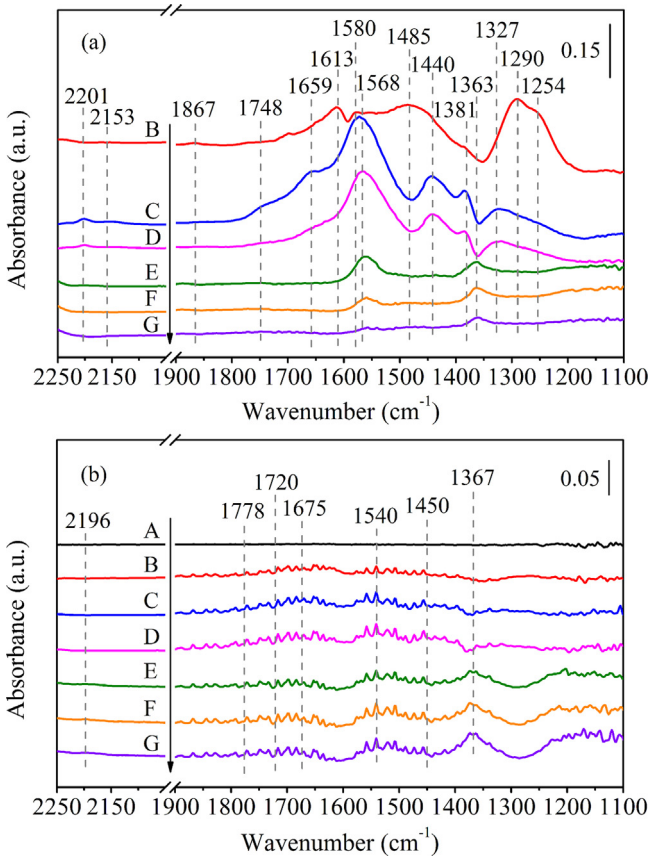

Fig. 10. *In situ* DRIFT spectra of the species formed during the C_3H_6-SCR reaction over Hy-Sample (a) and Co-Sample (b) at different temperatures. (A) 0 min at 25 °C, (B) 25 °C, (C) 150 °C, (D) 200 °C, (E) 250 °C, (F) 275 °C and (G) 300 °C.

reaction temperature was increased to 150 °C, the primary surface adsorbed species were changed to be the partially oxidized hydrocarbons, including formate (1363 and 1381 cm^{-1}), acetate (1440 and 1568 cm^{-1}), enolic species (δ(CH) around 1327 cm^{-1}) and acetaldehyde (ν(C=O) around 1748 cm^{-1}) [4,55,56]. Due to the reaction with C_3H_6 and/or oxygenates, the intensity of the characteristic bands of nitrates was weakened. Meanwhile, some N-containing organic intermediates were generated, including organo-nitro R—ONO (ν(N=O) around 1657 cm^{-1}), —CN species (2157 cm^{-1}) and —NCO species (2201 cm^{-1}) [57]. The intensity of these characteristic bands assigned to oxygenates and N-containing organics was gradually decreased by raising the reaction temperature, which could be due to the acceleration of the reactions with nitrates. Moreover, the complete oxidation may also lead to some consumption of oxygenates.

For Co-Sample, the features of inorganic N-containing species were not significant due to the high noise (the S/N (RMS) of the spectra in the range of 2250–1100 cm^{-1} was around 1.52), thus the spectrum obtained at 0 min in the C_3H_6-SCR reaction at 25 °C were added as a control. After reaching the steady state at 25 °C (curve B), the characteristic peaks of adsorbed N_2O_4 (1675 cm^{-1}) and NO_2 (1720 cm^{-1}) with low intensities were observed [48], while no nitrates was formed on the catalyst surface. By raising the reaction temperature, C_3H_6 was activated and the main derivatives were acetate (1450 and 1550 cm^{-1}), formate (1367 cm^{-1}) and acetone (1675 cm^{-1}) [53]. Considering the easy decomposition of dinitrosyls at high temperature, the band at 1778 cm^{-1} was assigned to ν(C=O) of carbonyl but not the feature of dinitrosyls [48,56]. By Comparison, C_3H_6 activation over Co-Sample was not as facile as that over Hy-Sample. The generation of oxygenates started at a much higher temperature of 250 °C, and the concentrations of them were pretty low. More importantly, the N-containing organic intermediates R—ONO, —CN and —NCO species were not generated over Co-Sample, which were considered as the important species to directly react with nitrates and/or NO_2 to produce N_2 [52,53,57]. Based on previous studies [27,51,52,58], —CN and —NCO species were generated by the direct reaction between oxygenates and inorganic N-containing surface species (nitrates and gas-phase NO_x) or *via* R—ONO compound, in which the formation of oxygenates deriving from C_3H_6 activation was always considered as a necessary and rate-determining step. Herein, the absence of N-containing organic species over Co-Sample was mainly caused by the weak capacity of catalyst toward the activation of C_3H_6 and NO.

Among the various proposed mechanisms about HC-SCR reaction, the hydrolysis of —NCO species has been widely accepted as a major pathway to yield N_2, in which NH_3 formed and subsequently reacted with inorganic N-containing surface species [52,59–61]. Though the role of —CN species in HC-SCR was still in debate over diverse catalysts, the —CN species have been confirmed as an important intermediate in Cu–Ti–Zr catalytic system for the C_3H_6-SCR reaction in our previous study, which produced N_2 by the reaction with nitrates and/or NO_2 [58]. Therefore, from the DRIFTS results it was suggested that the catalyst preparation method could significantly affect the formation and transformation of surface adsorbed intermediates. The excellent SCR activity of Hy-Sample was attributed to the efficient activation of reactants and the acceleration in the formation and reaction of N-containing organic intermediates.

4. Conclusions

A unique Cu-doped $Ti_{0.5}Zr_{0.5}O_{2-\delta}$ mixed oxide catalyst with hierarchical structure morphology was successfully fabricated using the hydrothermal method and was shown to exhibit excellent activity in the NO_x-SCR reaction with propylene. The superior performance of this catalyst was attributed to its uniform and well-organized morphology. However, these features had been destroyed when attempting to prepare the catalyst with the same precursors but using the co-precipitation method. The preparation method affected the physico-chemical properties of catalyst significantly. The hydrothermal method enhanced the efficient dispersion of CuO species on catalyst surface and promoted the formation of surface adsorbed oxygen, thus increased the quantity of active sites participating in the SCR reaction. These properties were shown to be beneficial for the acceleration of the adsorption and activation of the reactants NO and C_3H_6, and the interaction between their derivatives induced the formation of N-containing organic intermediates, including —CN, —NCO and R—ONO species, an important step for the generation of N_2. In contrast, the irregular aggregation of crystals in Co-Sample from the co-precipitation process resulted in the coating of CuO_x species in the interior of the material, causing a serious loss of efficient active sites. Consequently, the formation and transformation of intermediates were suppressed in the SCR reaction and a poor activity was observed over Co-Sample. The findings of this work offer a direct correlation between the catalytic performances and the corresponding surface chemistry and structure, which could be optimized by employing appropriate synthesis methods.

References

[1] X.Y. Li, L. Guang, Z.P. Qu, D.K. Zhang, S.M. Liu, Appl. Catal. A: Gen. 398 (2011) 82–87.
[2] W. Yang, R. Zhang, B. Chen, D. Duprez, S. Royer, Environ. Sci. Technol. 46 (2012) 11280–11288.

[3] A. Iglesias-Juez, A. Martínez-Arias, M. Fernández-García, J. Catal. 221 (2004) 148–161.
[4] T. Gu, R. Jin, Y. Liu, H. Liu, X. Weng, Z. Wu, Appl. Catal. B: Environ. 129 (2013) 30–38.
[5] F. Seyedeyn-Azad, D.K. Zhang, Catal. Today 68 (2001) 161–171.
[6] T. Boningari, R. Koirala, P.G. Smirniotis, Appl. Catal. B: Environ. 127 (2012) 255–264.
[7] R. Gao, D. Zhang, P. Maitarad, L. Shi, T. Rungrotmongkol, H. Li, J. Zhang, W. Cao, J. Phys. Chem. C 117 (2013) 10502–10511.
[8] P. Gao, F. Li, H. Zhan, N. Zhao, F. Xiao, W. Wei, L. Zhong, H. Wang, Y. Sun, J. Catal. 298 (2013) 51–60.
[9] F. Bin, C. Song, G. Lv, J. Song, S. Wu, X. Li, Appl. Catal. B: Environ. 150–151 (2014) 532–543.
[10] J. Liu, X. Li, Q. Zhao, D. Zhang, Catal. Sci. Technol. 2 (2012) 1711–1718.
[11] S. Watanabe, X. Ma, C. Song, J. Phys. Chem. C 113 (2009) 14249–14257.
[12] C. Sun, J. Zhu, Y. Lv, L. Qi, B. Liu, F. Gao, K. Sun, L. Dong, Y. Chen, Appl. Catal. B: Environ. 103 (2011) 206–220.
[13] P.E. Lippens, A.V. Chadwick, A. Weibel, R. Bouchet, P. Knauth, J. Phys. Chem. C 112 (2008) 43–47.
[14] K. Ito, S. Kakino, K. Ikeue, M. Machida, Appl. Catal. B: Environ. 74 (2007) 137–143.
[15] J. Liu, X. Li, Q. Zhao, C. Hao, S. Wang, M. Tadé, ACS Catal. 4 (2014) 2426–2436.
[16] R. Zhang, W.Y. Teoh, R. Amal, B. Chen, S. Kaliaguine, J. Catal. 272 (2010) 210–219.
[17] S. Roy, B. Viswanath, M.S. Hegde, G. Madras, J. Phys. Chem. C 112 (2008) 6002–6012.
[18] K.A. Headon, D.K. Zhang, Dev. Chem. Eng. Mineral Process 6 (1998) 9–20.
[19] K.A. Headon, D.K. Zhang, Ind. Eng. Chem. Res. 36 (1997) 4595–4599.
[20] C.C. Chusuei, M.A. Brookshier, D.W. Goodman, Langmuir 15 (1999) 2806–2808.
[21] H. Yahiro, M. Iwamoto, Appl. Catal. A: Gen. 222 (2001) 163–181.
[22] F. Liu, H. He, J. Phys. Chem. C 114 (2010) 16929–16936.
[23] Z.Y. Fei, B. Sun, L. Zhao, W.J. Ji, C.T. Au, Chem. Eur. J. 19 (2013) 6480–6487.
[24] L. Zhang, L. Shi, L. Huang, J. Zhang, R. Gao, D. Zhang, ACS Catal. 4 (2014) 1753–1763.
[25] E.I. Vovk, A. Turksoy, V.I. Bukhtiyarov, E. Ozensoy, J. Phys. Chem. C 117 (2013) 7713–7720.
[26] J. Liu, X. Li, Q. Zhao, D. Zhang, N. Pancras, J. Mol. Catal. A: Chem. 378 (2013) 115–123.
[27] M. Haneda, Y. Kintaichi, M. Inaba, H. Hamada, Catal. Today (1998) 127–135.
[28] L. Torrente-Murciano, A. Gilbank, B. Puertolas, T. Garcia, B. Solsona, D. Chadwick, Appl. Catal. B: Environ. 132–133 (2013) 116–122.
[29] C. Zhang, J. Lin, Phys. Chem. Chem. Phys. 13 (2011) 3896–3905.
[30] S.A. Yashnik, A.V. Salnikov, N.T. Vasenin, V.F. Anufrienko, Z.R. Ismagilov, Catal. Today 197 (2012) 214–227.
[31] S.S.R. Putluru, A. Riisager, R. Fehrmann, Appl. Catal. B: Environ. 101 (2011) 183–188.
[32] K. Chaudhari, R. Bal, D. Srinivas, A.J. Chandwadkar, S. Sivasanker, Microporous Mesoporous Mater. 50 (2001) 209–218.
[33] M. Fernández-García, A. Martínez-Arias, A.B. Hungría, A. Iglesias-Juez, J.C. Conesa, J. Soria, Phys. Chem. Chem. Phys. 4 (2002) 2473–2481.
[34] S. Zhu, X. Gao, Y. Zhu, Y. Zhu, H. Zheng, Y. Li, J. Catal. 303 (2013) 70–79.
[35] M. Shen, M. Yang, J. Wang, J. Wen, M. Zhao, W. Wang, J. Phys. Chem. C 113 (2009) 3212–3221.
[36] M. Shen, J. Wang, Y. An, J. Wang, W. Wang, Phys. Chem. C 113 (2009) 1543–1551.
[37] W. Cai, J. Yu, S. Gu, M. Jaroniec, Cryst. Growth Des. 10 (2010) 3977–3982.
[38] S. Shang, X. Jiao, D. Chen, ACS Appl. Mater. Interfaces 4 (2012) 860–865.
[39] X. Jiang, T.L. Ward, Y.S. Cheng, J. Liu, C.J. Brinker, Chem. Commun. 46 (2010) 3019–3021.
[40] F.C. Meunier, R. Ukropec, C. Stapleton, J.R.H. Ross, Appl. Catal. B: Environ. 30 (2001) 163–172.
[41] T. Chaieb, L. Delannoy, C. Louis, C. Thomas, Appl. Catal. B: Environ. 142–143 (2013) 780–784.
[42] C. Zhang, H. He, Y. Yu, Catal. Today 90 (2004) 191–197.
[43] K. Shimizu, A. Satsuma, T. Hattori, Appl. Catal. B: Environ. 25 (2000) 239–247.
[44] J. Pérez-Ramírez, J.M. Garćia-Cortés, F. Kapteijn, G. Mul, J.A. Moulijn, C.S. de Lecea, Appl. Catal. B: Environ. 29 (2001) 285–298.
[45] T.T. Yang, H.T. Bi, X.X. Cheng, Appl. Catal. B: Environ. 102 (2011) 163–171.
[46] K. Ralphs, C. D'Agostino, R. Burch, S. Chansai, L.F. Gladden, C. Hardacre, S.L. James, J. Mitchell, S.F.R. Taylor, Catal. Sci. Technol. 4 (2014) 531–539.
[47] L. Zhang, J. Pierce, V.L. Leung, D. Wang, W.S. Epling, J. Phys. Chem. C 117 (2013) 8282–8289.
[48] K.I. Hadjiivanov, Catal. Rev. 42 (2000) 71–144.
[49] I. Sobczak, M. Ziolek, M. Nowacka, Microporous Mesoporous Mater. 78 (2005) 103–116.
[50] K. Shimizu, A. Satsuma, Phys. Chem. Chem. Phys. 8 (2006) 2677–2695.
[51] P. Pietrzyk, C. Dujardin, K. Góra-Marek, P. Granger, Z. Sojka, Phys. Chem. Chem. Phys. 14 (2012) 2203–2215.
[52] S. Tamm, H.H. Ingelsten, A.E.C. Palmqvist, J. Catal. 255 (2008) 304–312.
[53] L.Q. Nguyen, C. Salim, H. Hinode, Appl. Catal. B: Environ. 96 (2010) 299–306.
[54] R. Jin, Y. Liu, Y. Wang, W. Cen, Z. Wu, H. Wang, X. Weng, Appl. Catal. B: Environ. 148–149 (2014) 582–588.
[55] Y. Yan, Y. Yu, H. He, J. Zhao, J. Catal. 293 (2012) 13–26.
[56] Y. Yu, H. He, Q. Feng, H. Gao, X. Yang, Appl. Catal. B: Environ. 49 (2004) 159–171.
[57] Y. Yu, X. Zhang, H. He, Appl. Catal. B: Environ. 75 (2007) 298–302.
[58] J. Liu, X. Li, Q. Zhao, C. Hao, D. Zhang, Environ. Sci. Technol. 47 (2013) 4528–4535.
[59] J.L. Flores-Moreno, G. Delahay, F. Figueras, B. Coq, J. Catal. 236 (2005) 292–303.
[60] N. Bion, J. Saussey, M. Haneda, M. Daturi, J. Catal. 217 (2003) 47–58.
[61] H.H. Ingelsten, M. Skoglundh, Catal. Lett. 106 (2006) 15–19.